Inorganic Chemistry

pubs.acs.org/IC Article

Reversible C−C Bond Formation, Halide Abstraction, and Electromers in Complexes of Iron Containing Redox-Noninnocent Pyridine-imine Ligands

Devika Pokhriyal, Spencer P. Heins, Renee J. Sifri, Dillon T. Gentekos, Rachael E. Coleman, Peter T. Wolczanski,* Thomas R. Cundari, Brett P. Fors, Kyle M. Lancaster, and Samantha N. MacMillan

Cite This: *Inorg. Chem.* 2021, 60, 18662−18673 Read Online

ABSTRACT: The exploration of pyridine-imine (PI) iron complexes that exhibit redox noninnocence (RNI) led to several interesting discoveries. The reduction of (PI)FeX_2 species afforded disproportionation products such as $(dmpPI)_2FeX$ (dmp = 2,6-Me_2-C_6H_3, X = Cl, Br; **8**-X) and $(dippPI)_2FeX$ (dipp = 2,6-$^iPr_2$-C_6H_3, X = Cl, Br; **9**-X), which were independently prepared by reductions of (PI)FeX_2 in the presence of PI. The crystal structure of **8**-Br possessed an asymmetric unit with two distinct electromers, species with different electronic GSs: a low-spin (S = 1/2) configuration derived from an intermediate-spin S = 1 core antiferromagnetically (AF) coupled to an S = 1/2 PI ligand, and an S = 3/2 center resulting from a high-spin S = 2 core AF-coupled to an S = 1/2 PI ligand. Calculations were used to energetically compare plausible ground states. Polydentate diazepane-PI (DHPI) ligands were applied to the synthesis of monomeric dihalides (DHPI)FeX_2 (X = Cl, **1**-Cl_2; X = Br, **1**-Br_2); reduction generated the highly distorted bioctahedral dimers $(DHPA)_2Fe_2X_2$ ($(\mathbf{3}\text{-X})_2$) containing a C−C bond formed from imine coupling; the monomers **1**-X_2 could be regenerated upon Ph_3CX oxidation. Dihalides and their reduced counterparts were subjected to various alkyl halides and methyl methacrylate (MMA), generating polymers with little to no molecular weight control, indicative of simple radical-initiated polymerization.

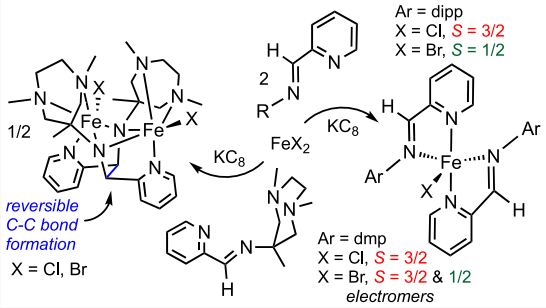

INTRODUCTION

Recent research in these laboratories has discovered numerous C−C bond forming processes in coordination complexes possessing redox-noninnocent ligands.[1−11] Figure 1 illustrates some highlights: (a) the formation of three new C−C bonds and six stereocenters about Cr, Co, and Ni metal−metal bonds,[1] (b) reversible and (c) irreversible azaallyl couplings,[2−6] and a nickel bis-pyridine-imine chelate complex with five ligand-localized redox states; degradation of the dianion (n = 2−) affords azacyclopentene rings.[7] Clearly subtle changes can differentiate species exhibiting redox noninnocence (RNI)[12−19] ascertained via metric changes and those that couple incipient radicaloids to generate C−C bonds.[1−11,20−22]

Previous investigations into $(AlkylN{=}CHpy)_2Fe(L/X_n)$ complexes[5] suggested that pyridine-imine (PI) dihalides would be excellent precursors for exploring stable redox-noninnocent (RNI) species and examining metric features in nonhomoleptic[23] systems. When these complexes were probed, electromers were discovered within an asymmetric unit of an X-ray crystal structure.[24,25] Related to spin-crossover species,[26] in which the predominance of high-spin and low-spin d^n variants is temperature-dependent, electromers differ in the distribution of electrons between the ligand and the metal. In addition to the standard PI complexes, a weak-field chelate of iron utilizing a multidentate diazepane-PI ligand was also investigated and discovered to undergo reversible C−C bond formation. This report provides evidence for the above, including high-level calculational and Mössbauer spectroscopic support.

RESULTS AND DISCUSSION

D(H/M)PI Syntheses. A nitro-Mannich reaction[27] featuring *N*,*N*-dimethylethylenediamine and nitroethane proceeds smoothly under solvent-free conditions to afford 1,4,6-trimethyl-6-nitro-1,4-diazepane, which is isolated in 50% yield after vacuum distillation (Scheme 1).[28] Hydrogenation

Received: June 15, 2021
Published: December 10, 2021

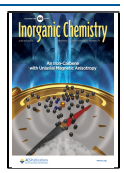

https://doi.org/10.1021/acs.inorgchem.1c01815
Inorg. Chem. 2021, 60, 18662−18673

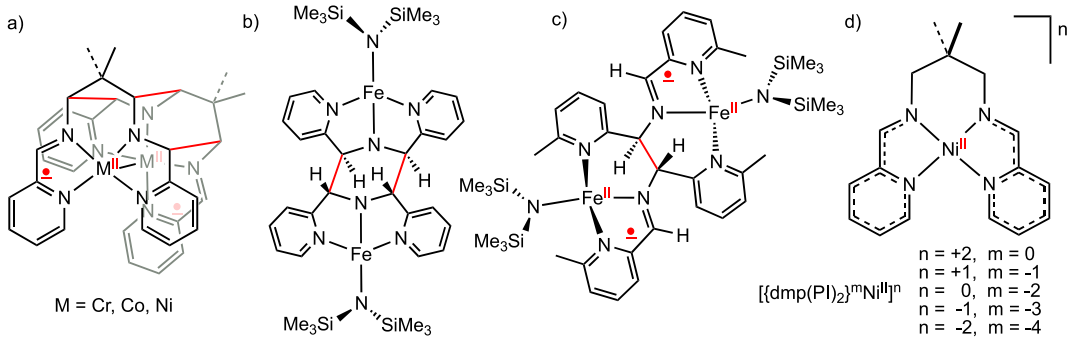

Figure 1. Redox noninnocence (RNI) in transition-metal azaallyl and pyridine-imine complexes: (a) three C−C bonds and six stereocenters generated; (b) two C−C bonds formed reversibly; (c) a C−C bond formed irreversibly; (d) a constrained bis-pyridine-imine chelate of Ni featuring five redox states.

Scheme 1. Diazepane-pyridineimine (R = H, DHPI; R = Me, DMPI) Syntheses

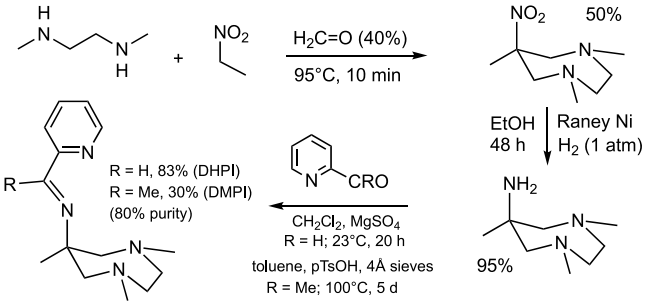

under Raney Ni conditions (EtOH, H_2 (1 atm)) afforded the corresponding amine as a clear liquid in near-quantitative yield. Its subsequent condensation with 2-pyridinecarboxaldehyde, using $MgSO_4$ as a dehydrating agent, generated the ligand (*E*)-1-(pyridin-2-yl)-N-(1,4,6-trimethyl-1,4-diazepan-6-yl)-methanimine (DHPI) as a viscous faint yellow oil in 83% yield. The switch to 2-acetylpyridine required quite harsh conditions, and the imine product (DMPI) was sensitive to reversion to the starting materials with any moisture present. Yields were typically low, and starting materials were present in ∼20% amounts, but their presence did not affect subsequent chelation efforts.

Synthesis of (DHPI)FeX$_2$ (X = Cl, 1-Cl$_2$; X = Br, 1-Br$_2$) and (DMPI)FeCl$_2$ (2-Cl$_2$). DHPI was added to a suspension of FeX_2 (X = Cl, Br) in THF, heated for 1 h, and cooled over a 12 h period to afford (DHPI)FeX_2 (X = Cl, **1**-Cl$_2$, 92%; X = Br, **1**-Br$_2$, 85%) as blue microcrystalline solids according to eq 1.

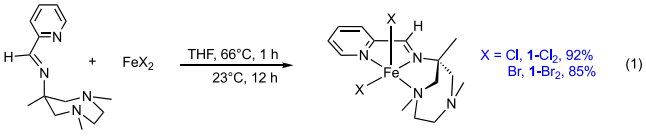

The ^{1}H NMR spectrum of **1**-Cl$_2$ displays 10 paramagnetically shifted resonances suggestive of a lack of symmetry, and structural evidence (*vide infra*) supported this claim, revealing a square-pyramidal geometry. The dibromide derivative **1**-Br$_2$ manifested 11 similarly shifted resonances and likely a related structure. Evans' method[29] solution magnetic moments on the dichloride (μ_{eff} = 5.0(1) μ_B) and the dibromide (μ_{eff} = 5.2(1) μ_B) are consistent with the expected high-spin S = 2 iron centers.

A similar reaction involving the DMPI ligand and $FeCl_2$ afforded another blue microcrystalline substance with related spectroscopic characteristics, but the structure of (DMPI)-$FeCl_2$ (**2**-Cl$_2$, 83%, eq 2) possessed a distorted-octahedral framework (*vide infra*). Evans' method[29] measurements of **2**-Cl confirmed its S = 2 core, as μ_{eff} = 5.0(1) μ_B.

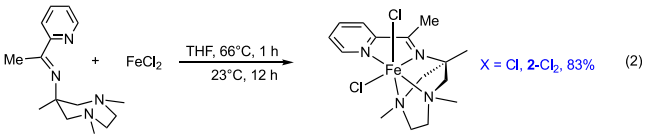

Structure of (DHPI)FeCl$_2$ (1-Cl$_2$). A molecular view of (DHPI)$FeCl_2$ (**1**-Cl$_2$) is given in Figure 2, along with pertinent

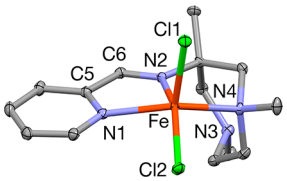

Figure 2. Molecular view of (DHPI)$FeCl_2$ (**1**-Cl$_2$). Selected interatomic distances (Å) and angles (deg): FeCl1, 2.3252(3); FeCl2, 2.3317(3); FeN1, 2.1634(10); FeN2, 2.1408(9); FeN3, 4.394(10); FeN4, 2.1842(10); N1−C5, 1.3398(15); C5−C6, 1.4722(15); N2−C6, 1.2742(15); Cl1−Fe−Cl2, 107.460(11); Cl1−Fe−N1, 107.30(3); Cl1−Fe−N2, 102.19(3); Cl1−Fe−N4, 100.66(3); Cl2−Fe−N1, 92.75(3); Cl2−Fe−N2, 150.08(3); Cl2−Fe−N4, 102.11(3); N1−Fe−N2, 74.44(4); N1−Fe−N4, 142.62(3); N2−Fe−N4, 75.81(3); Fe−N2−C6, 122.13(9); N2−C6−C5, 116.43(10); N1−C5−C6, 114.51(10); Fe−N1−C5, 115.22(7).

distances and angles. It has a distorted-square-pyramidal configuration with Cl1 in the apical position and an Addison parameter of $t \approx 0.12$.[30] The apical to basal angles average 104(3)° with a range of 107.460(11) (Cl1−Fe−Cl2) to 100.66(3)° (Cl1−Fe−N4). The core distances are clearly in line with a high-spin ferrous center, with Fe−N distances averaging 2.16(2) Å and d(Fe−Cl)$_{av}$ = 2.329(5) Å. The bite angle for the pyridine-imine is 74.44(4)°, and it is assigned a neutral charge on the basis of the imine double-bond (1.2742(15) Å) and C(sp^2)−C(sp^2) single-bond (1.4722(15) Å) distances.[23,31] The lone pair of the remaining diazepane nitrogen (N3) is directed away from iron at a distance of 4.394(10) Å.

Structure of (DMPI)FeCl$_2$ (2-Cl$_2$). As the molecular view in Figure 3 reveals, the Me substituent on the imine changes

https://doi.org/10.1021/acs.inorgchem.1c01815
Inorg. Chem. 2021, 60, 18662−18673

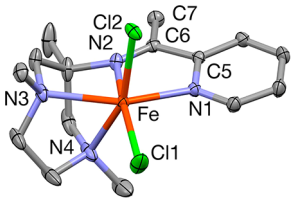

Figure 3. Molecular view of (DMPI)$FeCl_2$ (**2**-Cl_2). Selected interatomic distances (Å) and angles (deg): FeCl1, 2.3216(5); FeCl2, 2.4599(4); FeN1, 2.1626(13); FeN2, 2.1453(13); FeN3, 2.2919(13); FeN4, 2.3528(11); N1−C5, 1.335(2); C5−C6, 1.498(2); C6−C7, 1.503(2); N2−C6, 1.279(2); Cl1−Fe−Cl2, 101.78(2); Cl1−Fe−N1, 98.45(4); Cl1−Fe−N2, 161.59(4); Cl1−Fe−N3, 105.71(4); Cl1−Fe−N4, 94.35(5); Cl2−Fe−N1, 87.23(4); Cl2−Fe−N2, 94.54(4); Cl2−Fe−N3, 91.42(3); Cl2−Fe−N4, 158.72(4); N1−Fe−N2, 73.67(5); N1−Fe−N3, 155.55(5); N1−Fe−N4,104.17(5); N2−Fe−N3, 82.11(5); N2−Fe−N4, 72.19(3); N3−Fe−N4, 70.71(5); Fe−N2−C6, 120.82(10); N2−C6−C5, 113.27(13); N1−C5−C6, 114.91(13); Fe−N1−C5, 115.50(10).

the coordination to a distorted octahedron, although it is not clear why, as the bite angle of the PI ligand differs from that of **1**-Cl_2 by less than 1° (73.67(5)°). The diazepane nitrogens bind at distances of 2.2919(13) (N3) and 2.3528(11) (N4) Å, which are considerably longer than the 2.154(12) Å (average) distances of the PI nitrogens. The bite angles within the diazepane-imine face are 82.11(5)° (N2,N3), 72.19(3)° (N2,N4), and 70.71(5)° (N3,N4); hence, the distortion is quite evident, and *d*(FeCl2) is 2.4599(4) Å, almost 0.14 Å longer than *d*(FeCl1), perhaps suggesting that the *trans* influence of the trialkylamine, even if it is off-axis (Cl2−Fe−N4, 158.72(4)°), is appreciable.

C−C Bond Formation via Reductive Dimerization of (DHPI)FeX_2 (1-X_2, X = Cl, Br). The reduction of (DHPI)FeX_2 (**1**-X_2, X = Cl, Br) was attempted in order to test the unique diazepane-pyridineimine ligand for RNI. Treatment of **1**-Cl_2 with 1% Na/Hg or KC_8 in THF at −78 °C, followed by warming to 23 °C, caused a change in color from blue to red and a noted increase in solubility. After 60 h, a red product was precipitated via the addition of pentane, and a structural analysis revealed it to be the dimer $(DHPA)_2Fe_2Cl_2$ ((**3**-Cl)$_2$, 66%, $(DHPA)_2$ = 1,2-bis(pyridin-2-yl)-*N*1,*N*2-bis(1,4,6-trimethyl-1,4-diazepan-6-yl)ethane-1,2-diamide) (Scheme 2). The RNI of the DHPI ligand is not manifested via a reduced π-system but rather via C−C coupling of the imine functionality, likely due to radical character generated at the imine carbon upon reduction.[2,5,7,9,20−22] The bromide

Scheme 2. $(DHPA)_2Fe_2X_2$ ((3-X)$_2$) Preparation via C−C Coupling upon Reduction of 1-X_2

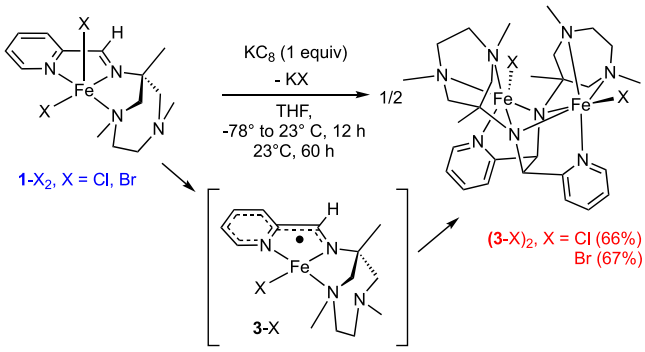

derivative can be similarly synthesized and isolated as a red powder in slightly higher yield (67%). The solution magnetic moments of (**3**-Cl)$_2$ and (**3**-Br)$_2$ were determined to be 7.4(2) and 7.8(1) μ_B, respectively, by Evans' method.[29] If the centers are not interacting, a spin-only value of 6.9 μ_B would be expected; hence, the greater number may be a consequence of spin−orbit contributions and/or minor ferromagnetic coupling between two high-spin (S = 2) iron centers. Repeated attempts to reduce the corresponding methyl-imine complex, (DMPI)-$FeCl_2$ (**2**-Cl_2) failed to elicit any tractable material. It is conceivable that the mere change of H for Me renders the C−C bond formation sterically difficult enough that the monomer, i.e. (DMPI)FeCl (**2**-Cl), persists long enough to degrade rather than dimerize. Attempts to obtain a tractable product generated from reduction proved futile.

Structure of $(DHPA)_2Fe_2Cl_2$ ((3-Cl)$_2$). A view of the dimer $(DHPA)_2Fe_2Cl_2$ ((**3**-Cl)$_2$) is given in Figure 4, along with

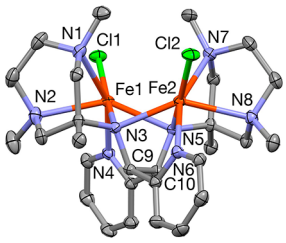

Figure 4. Molecular view of $(DHPA)_2Fe_2Cl_2$ ((**3**-Cl)$_2$). Selected interatomic distances (Å) and angles (deg): Fe1−Fe2, 3.131(2); Fe1−Cl1, 2.3536(5); Fe1−N1, 2.441(2); Fe1−N2, 2.484(2); Fe1−N3, 2.0310(15); Fe1−N4, 2.1717(15); Fe1−N5, 2.3544(15); Fe2−Cl2, 2.3605(5); Fe2−N3, 2.3156(15); Fe2−N5, 2.0474(15); Fe2−N6, 2.1920(16); Fe2−N7, 2.456(2); Fe2−N8, 2.467(2); Cl1−Fe−N1, 91.47(4); Cl−Fe1−N2, 99.67(4); Cl1−Fe−N3, 166.93(4); Cl1−Fe−N4, 91.33(4); Cl1−Fe1−N5, 116.67(4); N1−Fe1−N2, 67.89(6); N1−Fe1−N3, 76.29(6); N1−Fe1−N4, 157.85(6); N1−Fe1−N5, 123.26(6); N2−Fe1−N3, 117.02(6); N2−Fe1−N4, 80.15(6); N2−Fe1−N5, 140.22(6); N3−Fe1−N4, 101.73(6); N3−Fe1−N5, 68.10(6); N4−Fe1−N5, 74.38(6); Cl2−Fe2−N3, 117.02(4); Cl2−Fe2−N5, 167.08(5); Cl2−Fe2−N6, 91.06(4); Cl2−Fe2−N7, 92.39(4); Cl2−Fe2−N8, 98.78(4); N3−Fe2−N5, 68.65(6); N3−Fe2−N6, 74.47(6); N3−Fe2−N7, 122.73(4); N3−Fe2−N8, 140.54(4); N5−Fe2−N6, 101.78(6); N5−Fe2−N7, 75.19(4); N5−Fe2−N8, 80.07(4); N6−Fe2−N7, 157.71(4); N6−Fe2−N8, 89.65; N7−Fe2−N8, 68.06; C9−C10, 1.581(2).

selected metric parameters. A long C−C bond of 1.581(2) Å is obtained from imine coupling, which changes the imine nitrogens into asymmetrically bridging amides (*d*(FeN) = 2.04(1), 2.34(3) Å average) linking two irons that are 3.131(2) Å apart. Each iron core is a highly distorted octahedron, mostly a consequence of the small bite angles of the diazepane (68.0(2)°) and pyridine-amide chelate (74.43(6)°). The μ-N ligands are *trans* to the Fe−Cl bonds, which average 2.357(5) Å, and the iron-NMe bonds of the diazepane are quite long, averaging 2.46(2) Å. Only the Fe−N distances of the pyridines are normal at 2.182(14) Å. The long distances and distorted cores are consistent with the high-spin ferrous centers inferred from the magnetism.

The long 1.581(2) Å carbon−carbon bond formed upon dimerization has an energy of roughly 70 kcal/mol according to a BDE vs *d*(CC) correlation,[32] suggesting that it may be broken if sufficient enthalpic compensation can be provided. As shown in Scheme 3, treatment of the dimer $(DHPA)_2Fe_2Cl_2$ (**3**-Cl)$_2$ with stoichiometric trityl chloride or

https://doi.org/10.1021/acs.inorgchem.1c01815
Inorg. Chem. 2021, 60, 18662−18673

Scheme 3. Scission of the C−C Bond Induced by Ph_3CX (X = Cl, Br)

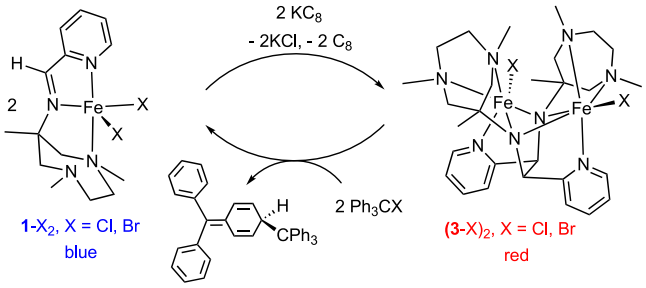

of the bromide dimer $(\mathbf{3}\text{-Br})_2$ with Ph_3CBr caused the immediate reversion from red to blue, as the corresponding monomeric dihalides $(DHPI)_2FeX_2$ ($\mathbf{1}\text{-X}_2$, X = Cl, Br) were generated. After 24 h, precipitation was complete, and Gomberg's dimer $(Ph_3C)_2$ and the dihalides were identified by ^{1}H NMR spectroscopy.

Reduction of $[(2\text{-py-CH}{=}\text{N-R})FeX]_2(\mu\text{-X})_2$. The C−C bond formation in $(DHPA)_2Fe_2X_2$ $(\mathbf{3}\text{-X})_2$ prompted a consideration of similar bond-forming events in well-studied $[(RPI)FeX]_2(\mu\text{-X})_2$ complexes;[16] thus, a select few were investigated. Using established procedures or simple variants[5,22,23,33,34] $[(RPI)FeX]_2(\mu\text{-X})_2$ (RPI = dmp = 2-py-CH═N(2,6-Me_2-C_6H_3), X = Cl, Br, **4**-X; RPI = dipp = 2-py-CH═N(2,6-^{i}Pr_2-C_6H_3), X = Cl, Br, **5**-X; RPI = 2-py-CH═NAd, X = Cl, Br, **6**-X; RPI = 2-py-CH═N^{c}Hex, X = Cl, **7**-Cl) were prepared by mixing 1 equiv of the pyridine-imine with ferrous chloride or bromide. As expected, the new cyclohexyl and adamantyl species possessed the same solubility properties as those previously prepared[33] and are described as dimers in eqs 3 and 4.

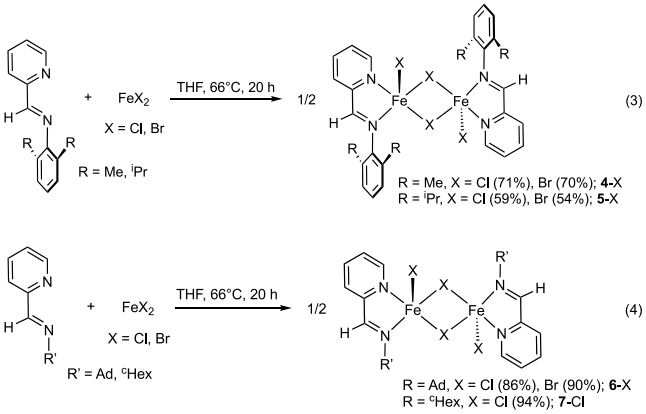

With the appropriate starting materials in hand, the 2,6-dimethylphenyl (dmp) dichlorides and dibromides $[(dmpPI)FeX]_2(\mu\text{-X})_2$ (X = Cl, **4**-Cl; X = Br, **4**-Br) were selected for reduction with KC_8. While the expected product was a solvated monopyridinediamine species, disproportionation was evident, and monomeric bis-PI complexes, $(dmpPI)_2FeX$ (X = Cl, **8**-Cl; X = Br, **8**-Br), were generated.[5] Once the course of the reaction was discerned, the reductions of **4**-X were conducted in the presence of 1 equiv of pyridine-imine in order to improve the yields, as shown in Scheme 4. Alternatively, FeX_2 was treated with the requisite 2 equiv of pyridine-imine and 1 equiv of KC_8 without the need for prior complexation of the chelate,[5] as eq 5 indicates. The diisopropylphenyl- and adamantyl-pyridine-imine derivatives (i.e., $(dippPI)_2FeX$ (X =

Scheme 4. Disproportionation upon Reduction of PI Dihalides 4-Cl and 4-Br

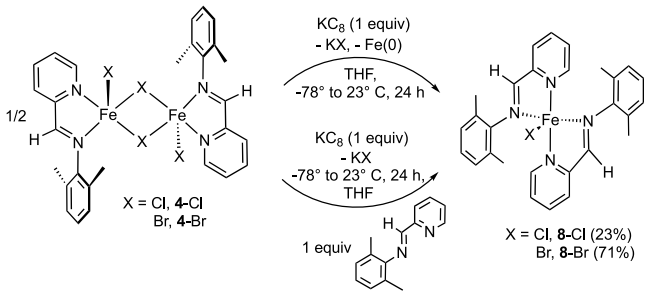

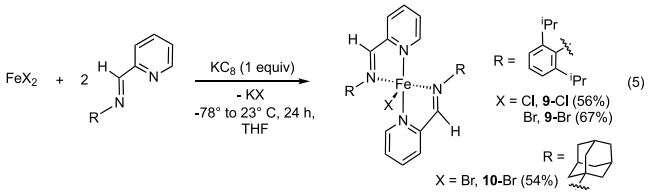

Cl, **9**-Cl; X = Br, **9**-Br) and $(AdPI)_2FeBr$ (**10**-Br)) were readily prepared in this fashion. The μ_{eff} values obtained for **8**-Cl (3.8 μ_B), **8**-Br (4.0 μ_B), **9**-Cl (3.7 μ_B), and **9**-Br (3.8 μ_B) were those of an S = 3/2 center as expected for Fe(I) but were more likely complicated by redox noninnocence involving the PI ligands,[5,23,35] as calculations suggest.

Unlike the diazepane-pyridineimine cases, no C−C bond formations were observed in reductions of the various dihalides described by Scheme 4 and eq 5. These compounds did serve as radical initiators in the polymerization of methyl methacrylate (MMA), as illustrated in Scheme 5. Whether

Scheme 5. Polymerization of Methyl Methacrylate Initiated by Various Halides in Combination with Various Halides, Including Some That Exhibit RNI

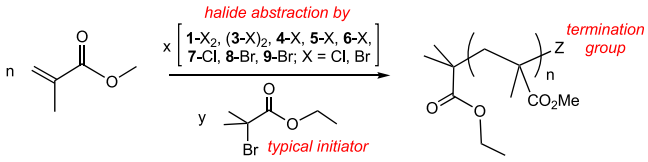

the halides were the sole initiators or were in combination (e.g., $\mathbf{1}\text{-Cl}_2$ and $(\mathbf{3}\text{-Cl})_2$), polymerization of MMA was noted, presumably due to halide abstraction as the initiation step, followed by propagation, etc.[36−45] See the Supporting Information for experimental details.

Structure of $(dmpPI)_2FeBr$ (8-Br). Figure 5 illustrates molecular views of the two molecules of $(dmpPI)_2FeBr$ (**8**-Br) that are found in the asymmetric unit. Core metric parameters are given in Table 1, which reveals distinct differences between the two, referred to as Fe1 and Fe2. In Fe1, the two Fe−N(py) and one Fe−N(im) distance average 2.13(3) Å, while the remaining Fe1−N14 distance is roughly ∼0.1 Å shorter at 2.0144(19) Å. The N13,N14-pyridine imine possesses bond distances of a neutral ligand in comparison to its partner (N11,N12), which corresponds more closely to a radical anion: $d(N_{im}C_{im})$ = 1.330(3) Å, $d(C_{im}C_{py})$ = 1.406(4) Å, $d(N_{py}C_{py})$ = 1.373(13) Å. This conclusion is based on the interpretations of Wieghardt et al. for neutral (0), anionic (1−), and dianionic (2−) pyridine-imines: d(N(im)−C(im)) = 1.28 Å (0), 1.34 Å (1−), 1.46 Å (2−); d(C(im)−C(py)) =

https://doi.org/10.1021/acs.inorgchem.1c01815
Inorg. Chem. 2021, 60, 18662−18673

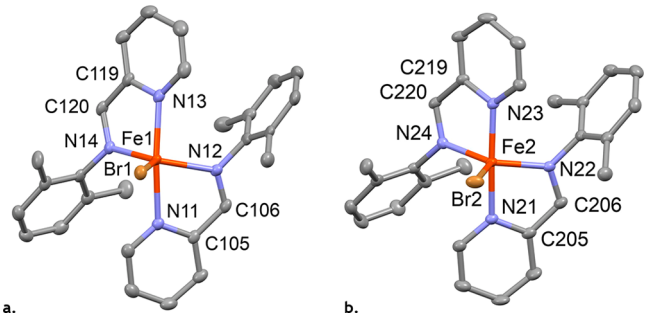

Figure 5. Views of high-spin (S = 3/2, a) and low-spin (S = 1/2, b) molecules of $(dmpPI)_2FeBr$ (**8**-Br) found in the asymmetric unit. Metric parameters are given in Table 1.

1.47 Å (0), 1.41 Å (1−), 1.35 Å (2−); d(N(py)−C(py)) = 1.35 Å (0), 1.39 Å (1−), 1.40 Å (2−)).[23] The core Fe1 is assigned to an Fe(II) center coupled to a PI radical anion, and the total charge on the PI ligands is roughly 1.0− on the basis of the Wieghardt data. Calculations agree with the charge evaluation, but the detailed electronic structure is atypical (*vide infra*).

While the two molecules are distorted trigonal pyramids, they are significantly different. The core Fe1 possesses a τ value of 0.64, whereas the center of Fe2 has τ = 0.70.[30] For the former, the pseudoaxial pyridine nitrogens are 162.60(7)° apart, and angles in the pseudoequatorial plane are fairly regular at ∼117, ∼117, and ∼125°. The higher τ value for Fe2 derives from a straighter N(py)−Fe2−N(py) angle of ∼173°, despite a slightly less regular trigonal plane (∼117, ∼113, ∼130°). The major difference in Fe2 is its average d(Fe−N) value of 1.946(14) Å, a considerable shortening from Fe1 by 0.05−0.20 Å and a distance more commensurate with lower-spin $(PI)_2FeL$ complexes.[5] Using a linear fit to Wieghardt's pyridine-imine parameters,[23] the PI ligands on Fe2 add up to a rough overall charge of 1.5−, a value that is consistent with calculations.

Structure of $(dippPI)_2FeBr$ (9-Br). Figure 6 gives a molecular view of $(dippPI)_2FeBr$ (**9**-Br), whose τ = 0.69[30] is closer to the lower-spin (S = 1/2) electromer of $(dmpPI)_2FeBr$ (**8**-Br). The metric parameters of **9**-Br, given in the caption of the figure, show a strong parallel with Fe2 in Figure 5, including pyridine-imine distances that are closer to radical anions, but may be disordered/average versions of a neutral

Table 1. Comparison of Metric Parameters for Fe1 and Fe2 Electromers of $(dmpPI)_2FeBr$ (8-Br) and Related Computed Bond Lengths (Å) and Angles (deg) Assigned to the Three Spin States S = 1/2, 3/2, 5/2[a]

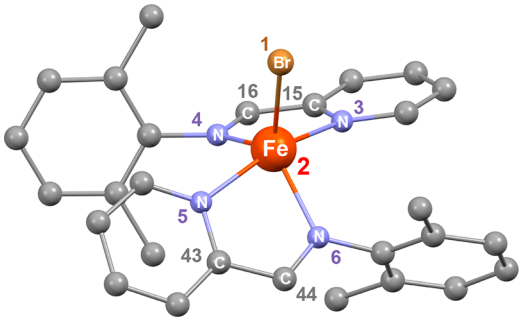

d/angle	no.	Fe1, τ = 0.64	Fe2, τ = 0.70	S = 1/2, τ = 0.73	S = 3/2 (AF), τ = 0.61	S = 5/2, τ = 0.53
Fe−Br	1−2	2.4409(4)	2.4518(4)	2.48	2.43	2.44
Fe−N(py)	2−3	2.1689(19)	1.9388(19)	1.96	2.24	2.21
Fe−N(im)	2−4	2.117(2)	1.9424(19)	2.04	2.16	2.21
Fe−N(py)	2−5	2.115(2)	1.9360(19)	1.96	2.23	2.21
Fe−N(im)	2−6	2.0144(19)	1.9672(18)	2.03	2.16	2.21
N(im)−C(im)	4−16	1.281(3)	1.325(3)	1.32	1.30	1.31
	6−44	1.330(3)	1.316(3)			
C(im)−C(py)	15−16	1.453(4)	1.413(4)	1.42	1.44	1.44
	43−44	1.406(4)	1.411(3)			
N(py)−C(py)	3−15	1.356(3)	1.370(3)	1.37	1.36	1.37
	5−43	1.373(13)	1.376(3)			
Br−Fe−N(py)	1−2−3	94.72(5)	94.52(6)	92.5	101.1	102.1
Br−Fe−N(im)	1−2−4	117.45(5)	116.68(5)	114.2	119.0	117.5
Br−Fe−N(py)	1−2−5	102.66(5)	92.85(5)	92.7	101.4	102.4
Br−Fe−N(im)	1−2−6	117.63(6	112.95(6)	114.9	119.9	118.5
N(py)−Fe−N(im)	3−2−4	75.32(8)	80.60(8)	80.4	75.2	75.7
N(py)−Fe−N(py)	3−2−5	162.60(7)	172.62(8)	174.8	157.5	155.5
N(py)−Fe−N(im)	3−2−6	94.05(7)	97.16(8)	97.4	93.6	92.7
N(im)−Fe−N(py)	4−2−5	95.71(8)	95.79(8)	97.4	93.6	92.7
N(im)−Fe−N(im)	4−2−6	124.51(8)	130.35(8)	130.9	121.1	124.0
N(py)−Fe−N(im)	5−2−6	78.61(8)	80.22(8)	80.5	75.2	75.8

[a]Black numbers refer to the atom labels from Figure 6, and colored numbers refer to computed atoms. Incorporating the B3LYP/6-311+G(d) derived entropic and enthalpic corrections yields $\Delta H°$ = 0.74 kcal/mol, $\Delta S°$ = −11.34 cal/(mol K), and $\Delta G°$ = 4.12 kcal/mol for the hypothetical equilibrium between the lower energy quartet configuration and the doublet geometry (Figure 7).

https://doi.org/10.1021/acs.inorgchem.1c01815
Inorg. Chem. 2021, 60, 18662−18673

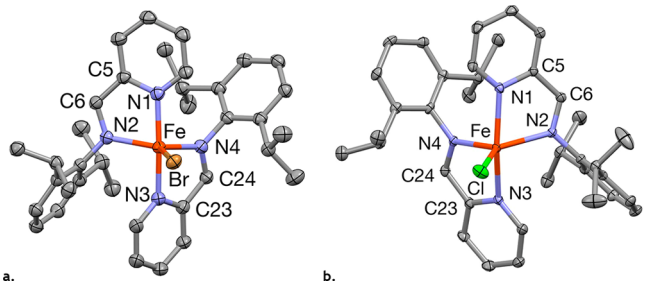

Figure 6. (a) Molecular view of $(dippPI)_2FeBr$ (**9**-Br; S = 1/2). Selected metrics (Å, deg): Fe−Br, 2.4315(3); Fe−N1, 1.9614(17); Fe−N2, 1.9662(14); Fe−N3, 1.9657(16); Fe−N4, 1.9656(14); N1−C5, 1.375(2); C5−C6, 1.414(2); N2−C6, 1.323(2); N3−C23, 1.373(2); C23−C24, 1.417(2); N4−C24, 1.319(2); Br−Fe−N1, 95.10(4); Br−Fe−N2, 115.95(4); Br−Fe−N3, 94.88(5); Br−Fe−N4, 115.35(4); N1−Fe−N2, 80.04(6); N1−Fe−N3, 170.02(7); N1−Fe−N4, 95.85(6); N2−Fe−N3, 95.57(6); N2−Fe−N4, 128.70; N3−Fe−N4, 79.83(6). (b) Molecular view of $(dippPI))_2FeCl$ (**9**-Cl; S = 3/2). Selected metrics (Å, deg): Fe−Cl, 2.2733(8); Fe−N1, 2.175(2); Fe−N2, 2.088(2); Fe−N3, 2.175(2); Fe−N4, 2.075(2); N1−C5, 1.365(2); C5−C6, 1.439(4); N2−C6, 1.297(3); N3−C23, 1.363(3); C23−C24, 1.435(4); N4−C24, 1.309(3); Cl−Fe−N1, 100.13(6); Cl−Fe−N2, 122.02(7); Cl−Fe−N3, 99.48(7); Cl−Fe−N4, 117.28(6); N1−Fe−N2, 75.74(8); N1−Fe−N3, 160.38(9); N1−Fe−N4, 94.25(9); N2−Fe−N3, 94.02(8); N2−Fe−N4, 120.70(9); N3−Fe−N4, 76.41(9).

and monoanionic (dippPI) ligand. As was stated above, the solution μ_{eff} value of **9**-Br is consistent with an S = 3/2 center, providing further curious aspects to this study.

Structure of $(dippPI)_2FeCl$ (9-Cl). Figure 6 also depicts a molecular view of $(dippPI)_2FeCl$ (**9**-Cl), whose τ = 0.66[30] is slightly closer to the higher-spin electromer of $(dmpPI)_2FeBr$ (**8**-Br). Metric parameters of **9**-Cl, given in the caption of the figure, show a strong parallel with Fe1 in Figure 5, including longer Fe−N distances more consistent with a higher spin configuration. In this instance the solid-state structure appears to parallel the solution μ_{eff} value that indicates an S = 3/2 spin system.

Calculations Relevant to $(RPI)_2FeBr$ (R = dmp, 8-Br; R = dipp, 9-Br). The distorted-tbp $(dmpPI)_2FeBr$ (**8**-Br) has two electronically distinct structures in its asymmetric unit, whereas only one of those is represented by the geometry of $(dippPI)_2FeBr$ (**9**-Br). As a nominal d^7 "Fe(I)" complex, geometry optimizations—initiated from the conformations in **8**-Br in Figure 5—were conducted on S = 5/2, 3/2 and 1/2 spin states, and the results are given in Table 1.

An inspection of computed and experimental bond lengths and angles for the inner core of **8**-Br strongly suggests that the Fe2 molecule is in the low-spin S = 1/2 state. An S = 3/2 state resulting from ferromagnetic coupling of an S = 1 core and a PI radical anion was deemed to be too high in energy; thus, its details are relegated to the Supporting Information. Differences among the S = 3/2 and 5/2 states are too minimal to make a confident assignment for Fe1; hence, calculations at the DLPNO-CCSD(T)/def2-TZVPP and MCSCF/6-31G(d) levels were conducted on smaller models, $(HPI)_2FeBr$ (**8H**-Br), the geometries of which were either derived from calculations (B3LYP/6-311+G(d) optimization) or experiment (manually replacing N-dmp with N−H) (Figure 7). Both geometries are similar, with the latter being C_1 and the former C_2. DLPNO-CCSD(T)/def2-TZVPP//B3LYP/6-311+G(d) calculations place the doublet and quartet states as ostensibly degenerate

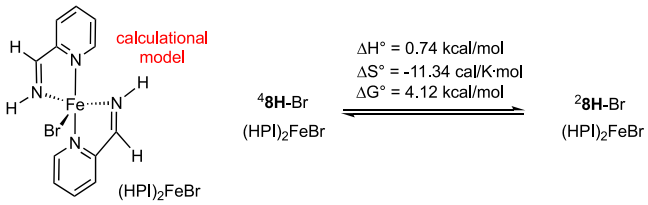

Figure 7. Calculated thermodynamic parameters for the equilibrium between the quartet state of the calculated model complex $(HPI)_2FeBr$ (^{4}**8H**-Br) and the nearby doublet, ^{2}**8H**-Br.

with the quartet lower in energy by 0.26 kcal/mol. The S = 5/2 state is noticeably higher than the predicted doublet ground state by 4.31 kcal/mol and was dismissed as a plausible Fe1 configuration. Incorporating the B3LYP/6-311+G(d) derived entropic and enthalpic corrections yields ΔH° = 0.74 kcal/mol, ΔS° = −11.34 cal/mol-K, and ΔG° = 4.12 kcal/mol for the hypothetical equilibrium between the lower energy quartet configuration and the doublet geometry (Figure 7).

The significant spin contamination found in the DFT calculations of **8**-Br hints at a complicated spin nature; thus, complete active space SCF (CASSCF) calculations were conducted on optimized models and those (**8H**-Br) generated from the crystal structure conformations. After experimenting with a variety of active space sizes, a CAS(9,9) active space was selected as optimal. For the Fe1 and Fe2 cores, the doublet and quartet states are close in energy, with that of the sextet being much higher. Given the structural congruence of the doublet with Fe2 (see Table 1), it is assigned a low-spin (S = 1/2) configuration derived from an intermediate-spin S = 1 core antiferromagnetically coupled to an S = 1/2 PI ligand: i.e., as $(HPI)(HPI)^{-\downarrow}Fe^{\uparrow\downarrow\uparrow\downarrow\uparrow\uparrow}Br$ and similarly for (dmpPI)-$(dmpPI)^{-\downarrow}Fe^{\uparrow\downarrow\uparrow\downarrow\uparrow\uparrow}Br$ (**8**-Br).

The related model complex ^{4}**8H**-Br is thus similarly construed as $(HPI)(HPI)^{-\downarrow}Fe^{\uparrow\downarrow\uparrow\uparrow\uparrow\uparrow}Br$, a high-spin S = 2 core antiferromagnetically coupled to an S = 1/2 PI ligand. By inference $(dmpPI)(dmpPI)^{-\downarrow}Fe^{\uparrow\downarrow\uparrow\uparrow\uparrow\uparrow}Br$ (**8**-Br) is accorded the same electronic configuration, as is the $(dippPI)_2FeBr$ (**9**-Br) derivative. The spin density of the S = 3/2 electromer is readily seen as greater than that of the S = 1/2 complement in the spin density plots illustrated in Figure 8.

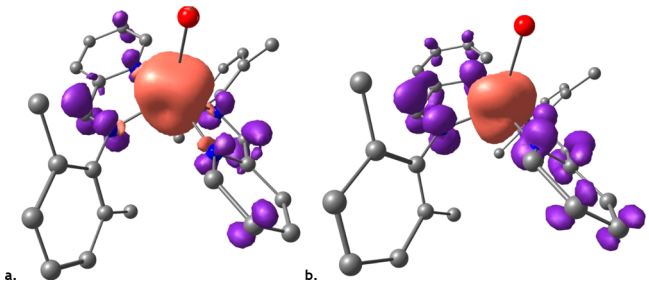

Figure 8. Spin density plots (isovalue 0.005 au) for the quartet (a, Fe1) and doublet (b, Fe2) electromers of $(dmpPI)_2FeBr$ (**8**-Br).

Mössbauer Studies on $(RPI)_2FeBr$ (8-Br, 9-Br). Figure 9 illustrates the Mössbauer spectrum of one crystalline sample of $(dmpPI)_2FeBr$ (**8**-Br), showing the two signals expected from the electromers observed in the structural study. On the basis of bond lengths,[46] the S_T = 1/2 complex calculated for Fe2 (Table 1) is assigned to the δ = 0.477(3) mm/s doublet with ΔE_Q = 1.077(6) mm/s (Γ = 0.295(8) mm/s). A broader

https://doi.org/10.1021/acs.inorgchem.1c01815
Inorg. Chem. 2021, 60, 18662−18673

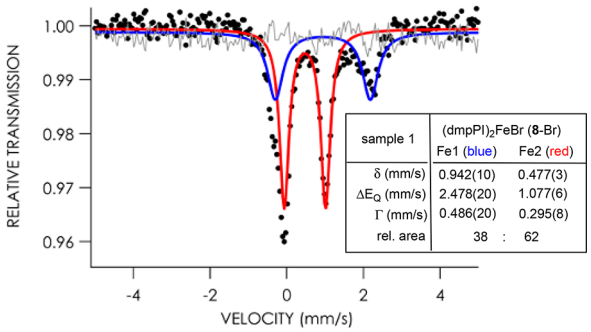

Figure 9. Mössbauer spectrum of solid $(dmpPI)_2FeBr$ (**8**-Br) collected at 85 K showing the $S = 1/2$ electromer (Fe2) in red and the $S = 3/2$ electromer (Fe1) in blue. A second, independently prepared sample had similar values at both 85 and 150 K (see Table 2). The residual (raw data minus fit) is shown in gray.

doublet at $\delta = 0.942(10)$ mm/s with $\Delta E_Q = 2.478(20)$ mm/s ($\Gamma = 0.486(20)$ mm/s) is assigned to Fe1 of **8**-Br, the quartet state electromer with longer bond distances. The broader signal for Fe1 is attributed to the vibrational anisotropy commonly observed in low-symmetry systems,[47,48] which is likely to be revealed in the higher-spin electromer with its longer bond distances. The relative areas of the $S = 1/2$ to $S = 3/2$ signals are roughly 60:40, and the data have been reproduced with an independently prepared sample, whose parameters are given in Table 2.

As for **8**-Br, when $(dippPI)_2FeBr$ (**9**-Br) is dissolved, only one species is seen by ^{1}H NMR spectroscopy, and Evans' method measurements[29] indicate it to be an $S = 3/2$ species. Its solid-state structure, which is akin to that of the $S = 1/2$ conformation found for Fe2 in **8**-Br, belies the solution data. Given the crystal structure parameters of **9**-Br, its Mössbauer spectrum was expected to conform to an $S = 1/2$ state. As Figure 10 reveals, the doublet at $\delta = 0.481(2)$ mm/s with $\Delta E_Q = 0.850(3)$ mm/s ($\Gamma = 0.266(4)$ mm/s) is remarkably close to those of the low-spin electromer of **8**-Br; hence, it is tentatively assigned the $(dippPI)(dippPI)^{-\downarrow}Fe^{\uparrow\downarrow\uparrow\uparrow\uparrow}Br$ (**9**-Br) configuration in the solid state.

To explore the possibility of other sets of electromers, a Mössbauer spectrum of $(dmpPI)_2FeCl$ (**8**-Cl) was obtained, and it is presented in Figure 11. As an indication of the subtle energy differences accorded the different spin state species, the modest change from Br to Cl elicits only a high-spin electromer. On this basis the chloride is predicted to have the $S = 3/2$ state derived from an $S = 2$ ferrous center antiferromagnetically coupled to an $S = 1/2$ PI ligand: i.e., $(dmpPI)(dmpPI)^{-\downarrow}Fe^{\uparrow\downarrow\uparrow\uparrow\uparrow}Cl$ (**8**-Cl). Likewise, the chloride $(dippPI)_2FeCl$ (**9**-Cl) was also investigated and found to possess parameters consistent with an $S = 3/2$ core, as given in Table 2. Once again, the weaker field chloride ligand was enough to generate the higher spin analogue $(dippPI)(dippPI)^{-\downarrow}Fe^{\uparrow\downarrow\uparrow\uparrow\uparrow}Cl$ (**9**-Cl). In addition, the Mössbauer spectrum of $[(dippPI)FeBr_2]_2$ (**5**-Br), a precursor to the RNI electromers, was also collected for comparison. As seen in Table 2, its parameters are distinct from those of the RNI bis-PI complexes are and fully consistent with its $S = 2$ high-spin center.[33]

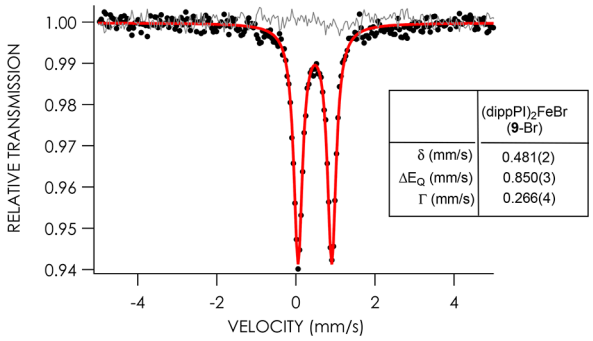

Figure 10. Mössbauer spectrum of solid $(dippPI)_2FeBr$ (**9**-Br) collected at 85 K consistent with an $S = 1/2$ configuration. The residual (raw data minus fit) is shown in gray.

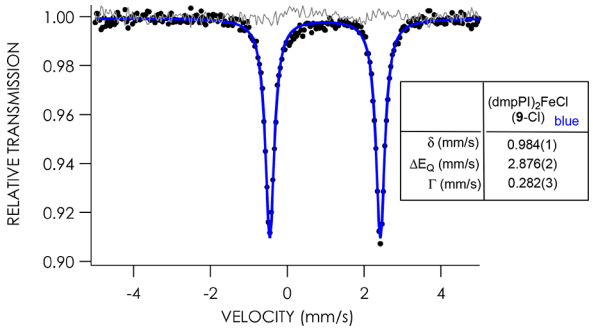

Figure 11. Mössbauer spectrum of solid $(dmpPI)_2FeCl$ (**8**-Cl) collected at 85 K consistent with an $S = 3/2$ configuration (blue). The residual (raw data minus fit) is shown in gray.

Calculations Pertaining to Halide Abstraction. Redox noninnocence (RNI) provides a ready explanation for why compounds that are formally "Fe(I)",[49−55] such as $(dmpPI)_2FeX$ (X = Cl, **8**-Cl; X = Br, **8**-Br) and $(dippPI)_2FeX$ (X = Cl, **9**-Cl; X = Br, **9**-Br), are relatively stable in comparison

Table 2. Bis-PI Iron Complex Mössbauer Parameters

entry	compd	T (K)	S	rel area	δ (mm/s)	ΔE_Q (mm/s)	Γ (mm/s)
1	$(dmpPI)_2FeBr$ (**8**-Br)	85	3/2	38	0.942(10)	2.478(20)	0.486(20)
		85	1/2	62	0.477(3)	1.077(6)	0.295(8)
2	$(dmpPI)_2FeBr$ (**8**-Br)[a]	85	3/2	39	0.927(6)	2.506(1)	0.444(16)
		85	1/2	61	0.474(2)	1.062(4)	0.282(5)
3	$(dmpPI)_2FeBr$ (**8**-Br)[a]	150	3/2	49	0.882(8)	2.177(1)	0.435(28)
		150	1/2	51	0.492(5)	1.014(10)	0.299(15)
4	$(dippPI)_2FeBr$ (**9**-Br)	85	1/2		0.481(2)	0.850(3)	0.266(4)
5	$(dmpPI)_2FeCl$ (**8**-Cl)	85	3/2		0.984(1)	2.876(2)	0.282(3)
6	$(dippPI)_2FeCl$ (**9**-Cl)	85	3/2		0.78(10)	2.426(20)	0.603(29)
7	$[(dippPI)FeBr_2]_2$ (**5**-Br)	85	2		1.049(3)	3.321(6)	0.322(9)

[a]Same sample.

https://doi.org/10.1021/acs.inorgchem.1c01815
Inorg. Chem. 2021, 60, 18662−18673

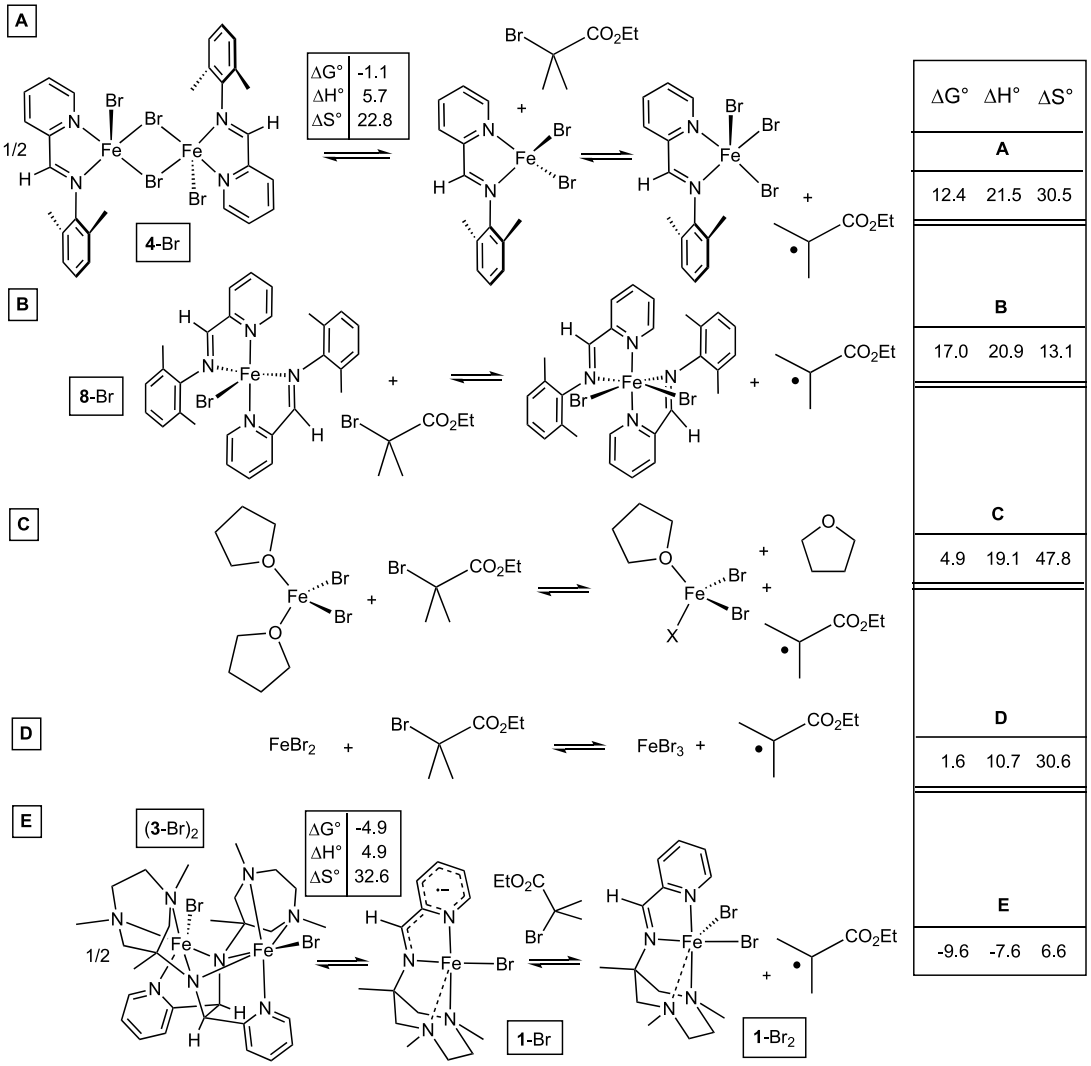

Figure 12. Calculated (ONIOM(b3pw91/6-311++G(d,p):UFF)) Br atom abstraction from ethyl bromoisobutyrate (EBI). The $\Delta G°$ and $\Delta H°$ values are given in kcal/mol, and the $\Delta S°$ values are given in cal/(mol K) (eu).

to their dihalide precursors. The RNI allows the complexes to be reformulated as "Fe(II)", a formal oxidation state that conveys stability. It is in this context that calculations regarding halide abstraction were conducted, to see if the thermodynamics were substantially affected by RNI.

Figure 12 depicts representative calculations involving bromide abstraction from ethyl bromoisobutyrate (EBI), a common initiator for methyl methacrylate polymerization as in Scheme 5. In **A**, bromide abstraction by (dmpPI)$FeBr_2$ (from the dimer **4**-Br) is shown to incur a substantial enthalpic penalty (21.5 kcal/mol) that is somewhat counteracted by the favorable entropy (30.5 eu) in generating the radical. In comparison with $(dmpPI)_2FeBr$ (**8**-Br, **B**), the complex that displays RNI, there is virtually no enthalpic difference (20.9 kcal/mol), indicative of the stability accorded the electron capture by the PI ligand. There is significantly less favorable entropy, as the crowding due to the increase in coordination number from 5 to 6 incurs a penalty. The lower entropy actually causes the abstraction in **A** to have a 4.6 kcal/mol lower free energy (12.4 vs 17.0 kcal/mol) than in **B**. It is likely that the loss of dmpPI would provide enough change such that both processes would be quite close. What is clear is that *possessing RNI provides no enthalpic advantage to halide abstraction* and that entropic factors can be complicated.

In **C** and **D**, simple bromide abstraction agents, $FeBr_2(THF)_2$ and $FeBr_2$, are revealed to have much lower free energies, 4.9 and 1.6 kcal/mol, respectively, than the ligated examples in **A** and **B**, but for different reasons. The enthalpy of Br abstraction for $FeBr_2(THF)_2$ to give $FeBr_3(THF)$ is 19.1 kcal/mol, similar to the previous cases, but loss of THF in the process affords a favorable entropy of 47.8 eu. For $FeBr_2$, conversion to $FeBr_3$ only incurs a 10.7 kcal/mol enthalpic change. Realistically, $FeBr_2$ needs to be solubilized to be effective, so that the more rational number for Br abstraction is that of $FeBr_2(THF)_2$, but it is informative that the simplest of coordination complexes is most effective.

For the diazepane dimer $(DHPA)_2Fe_2Br_2$ $(\mathbf{3}\text{-X})_2$, dissociation to a monomer is slightly favorable, and halide abstraction from EBI is favorable by −9.6 kcal/mol as well. In this system, despite RNI from the pyridine-imine ligand, the weakly coordinated amines of the DHPI ligand render **1**-Br sterically and electronically deficient, thereby permitting Br atom transfer from EBI to be significantly exoergic and likely explaining why the related stoichiometric Br atom transfer from Ph_3CBr was observed (Scheme 3).

https://doi.org/10.1021/acs.inorgchem.1c01815
Inorg. Chem. 2021, 60, 18662−18673

■ CONCLUSIONS

The reduction of pyridine-imine dihalide species led to bis-pyridine-imine halide species whose electronic features are subtly varied by the imine aryl substituent and halide. The most interesting example is $(dmpPI)_2FeBr$ (**8**-Br), which exists in a crystalline form as a mixture of electromers: one has an S = 1/2 configuration that arises from an intermediate-spin S = 1 core antiferromagnetically coupled to an S = 1/2 radical anion pyridine-imine ligand, i.e., $(dmpPI)(dmpPI)^{-\downarrow}Fe^{\uparrow\downarrow\uparrow\downarrow\uparrow\uparrow}Br$ (**8**-Br), and a second having an S = 3/2 configuration due to a high-spin S = 2 core antiferromagnetically coupled to an S = 1/2 radical anion pyridine-imine, i.e. $(dmpPI)(dmpPI)^{-\downarrow}Fe^{\uparrow\downarrow\uparrow\uparrow\uparrow\uparrow}Br$ (**8**-Br). Metric parameters and spin states from calculations dovetailed with the experimental results, and modest changes to aryl substituents and halide led to either the low-spin (2,6-^{i}Pr, Br^-) or high-spin (Cl^-) variants.

In an investigation of weak-field, mulitidentate diazepane-pyridineimine iron dihalides, five-coordinate ((DHPI)FeX_2 (X = Cl, **1**-Cl_2; X = Br, **1**-Br_2)) and six-coordinate ((DMPI)$FeCl_2$ (**2**-Cl_2)) species were found, and reductions of the latter generated highly distorted edge-shared bioctahedral complexes containing a C−C bond formed by imine coupling. Evidence of this roughly 70 kcal/mol bond being reversibly formed was obtained by oxidizing **1**-X_2 by trityl halide. For these derivatives, a C−C bond is the consequence of RNI, contrasting with the more conventional ligand charge state change of the simple PI ligands.

Given the C−C coupling in the diazepane-pyridineimine systems, it is perhaps puzzling why the simple PI complexes (e.g., **8**-X, **9**-X, X = Cl, Br) do not undergo a similar dimerization via C−C coupling, especially since these events have been seen in related compounds. First, note that dimerization incurs an entropic penalty of ∼20−30 eu ($T\Delta S°$ at 298 K 6−9 kcal/mol) and there is a stability conferred to formally "Fe(I)" compounds, redescribed as Fe(II) with redox-noninnocent ligands. This stability, and the favorable entropy of two monomers, is more favorable than the formation of a C−C bond and must be the situation for **8**-X and **9**-X. Using the rough estimate of favorable C−C bond formation in (**3**-Cl)$_2$ as ∼−70 kcal/mol and allowing for ∼−10 kcal/mol of disfavored entropic contribution, a crude estimate of RNI in **8**-X and **9**-X is ∼−30 kcal/mol per iron center. Note that several other interactions in (**3**-Cl)$_2$ are being ignored in this estimate.

Virtually all of the complexes can be used to initiate methyl methacrylate polymerization via Br atom abstraction. In calculated comparisons between iron dibromides and "Fe(I)" PI compounds possessing RNI, there is a negligible difference in the enthalpy of abstraction; hence, there appears to be no apparent advantage to having redox-active ligands for this purpose in these systems.

■ EXPERIMENTAL SECTION

General Synthesis and Characterization. All manipulations were performed using either glovebox or high-vacuum-line techniques. All glassware was oven-dried. THF and diethyl ether were distilled under nitrogen from purple sodium benzophenone ketyl and vacuum-transferred from the same prior to use. Hydrocarbon solvents were treated in the same manner with the addition of 1−2 mL/L of tetraglyme. Benzene-d_6 was dried over sodium, vacuum-transferred, and stored over activated 4 Å molecular sieves. THF-d_8 was dried over sodium and stored over purple sodium benzophenone ketyl.

NMR spectra were acquired using Mercury 300 MHz, INOVA 400 MHz, and Bruker AV III HD 500 MHz (equipped with a 5 mm BBO Prodigy cryoprobe) spectrometers. Chemical shifts are reported relative to benzene-d_6 (^{1}H δ 7.16; ^{13}C{^{1}H} δ 128.06), THF-d_8 (^{1}H δ 3.58; ^{13}C{^{1}H} δ 67.57), or acetonitrile-d_3 (^{1}H δ 1.94; ^{13}C{^{1}H} δ 1.32 or 118.26). NMR spectra were processed using MNova 12.0. Infrared spectra were recorded on a 20 Nicolet Avatar 370 DTGX spectrophotometer interfaced to an IBM PC (OMNIC software). Solutions μ_{eff} values were obtained by the Evans method.[29]

Structural Studies. Upon isolation, the crystals were covered in polyisobutenes and placed under a cold N_2 stream on the appropriate goniometer head. Low-temperature X-ray diffraction data were collected on a Rigaku XtaLAB Synergy diffractometer coupled to a Rigaku Hypix detector with either Mo Kα radiation (λ = 0.71073 Å) or Cu Kα radiation (λ = 1.54184 Å), from a PhotonJet microfocus X-ray source at 100 K. The diffraction images were processed and scaled using the CrysAlisPro software.

Mössbauer Spectroscopy. Mössbauer data were collected using a SEECo Resonant Gamma-Ray spectrometer (Model W304) in zero magnetic field. Samples were maintained at 85 K using a Janis Research Model SVT-400 Cryostat filled with liquid nitrogen. An Fe foil at room temperature was used to calibrate the velocity scale. Data were fit using the WMOSS software package, using theoretical model 3 to fit to quadrupole doublets. Data reported are the average of 201 Monte Carlo simulations, and uncertaintities were derived from the standard deviation of these simulations.

Experimental Details. All experimental details are provided in the Supporting Information.

■ ASSOCIATED CONTENT

Supporting Information

The Supporting Information is available free of charge at https://pubs.acs.org/doi/10.1021/acs.inorgchem.1c01815.

Experimental details of all procedures, spectroscopic data, X-ray crystallographic information pertaining to **1**-Cl_2 (CCDC-2076531), **2**-Cl_2 (CCDC-2076530), (**3**-Cl)$_2$ (CCDC-2076534), **8**-Br (CCDC-2076529), **9**-Br (CCDC-2076532), and **9**-Cl (CCDC-2076533), and details of the calculations (PDF)

Accession Codes

CCDC 2076529−2076534 contain the supplementary crystallographic data for this paper. These data can be obtained free of charge via www.ccdc.cam.ac.uk/data_request/cif, or by emailing data_request@ccdc.cam.ac.uk, or by contacting The Cambridge Crystallographic Data Centre, 12 Union Road, Cambridge CB2 1EZ, UK; fax: +44 1223 336033.

■ AUTHOR INFORMATION

Corresponding Author

Peter T. Wolczanski − *Department of Chemistry & Chemical Biology, Baker Laboratory, Cornell University, Ithaca, New York 14853, United States;* orcid.org/0000-0003-4801-0614; Email: ptw2@cornell.edu

Authors

Devika Pokhriyal − *Department of Chemistry & Chemical Biology, Baker Laboratory, Cornell University, Ithaca, New York 14853, United States*

Spencer P. Heins − *Department of Chemistry & Chemical Biology, Baker Laboratory, Cornell University, Ithaca, New York 14853, United States*

Renee J. Sifri − *Department of Chemistry & Chemical Biology, Baker Laboratory, Cornell University, Ithaca, New York 14853, United States*

Dillon T. Gentekos − *Department of Chemistry & Chemical Biology, Baker Laboratory, Cornell University, Ithaca, New York 14853, United States*

Rachael E. Coleman − *Department of Chemistry & Chemical Biology, Baker Laboratory, Cornell University, Ithaca, New York 14853, United States;* orcid.org/0000-0002-9877-4607

Thomas R. Cundari − *Department of Chemistry, CASCaM, University of North Texas, Denton, Texas 76201, United States;* orcid.org/0000-0003-1822-6473

Brett P. Fors − *Department of Chemistry & Chemical Biology, Baker Laboratory, Cornell University, Ithaca, New York 14853, United States*

Kyle M. Lancaster − *Department of Chemistry & Chemical Biology, Baker Laboratory, Cornell University, Ithaca, New York 14853, United States;* orcid.org/0000-0001-7296-128X

Samantha N. MacMillan − *Department of Chemistry & Chemical Biology, Baker Laboratory, Cornell University, Ithaca, New York 14853, United States;* orcid.org/0000-0001-6516-1823

Complete contact information is available at: https://pubs.acs.org/10.1021/acs.inorgchem.1c01815

Notes

The authors declare no competing financial interest.

■ ACKNOWLEDGMENTS

P.T.W. thanks the National Science Foundation for funding this work (CHE-1953884), as does T.R.C. for partial support through CHE-1953547, and for their support of the UNT CASCaM HPC cluster, upon which the reported simulations were performed, via grant CHE-1531468. B.P.F. thanks the National Science Foundation Center for Sustainable Polymers at the University of Minnesota, a Center for Chemical Innovation (CHE-1901635). K.M.L. acknowledges the Department of Energy Office of Science for funds towards the purchase of the Mössbauer spectrometer (DE-SC0013997). P.T.W., B.P.F., and K.M.L. also acknowledge the support of Cornell University.

■ REFERENCES

(1) Hulley, E. B.; Wolczanski, P. T.; Lobkovsky, E. B. Carbon-carbon Bond Formation from Azaallyl and Imine Couplings About Metal-metal Bonds. *J. Am. Chem. Soc.* **2011**, *133*, 18058−18061.

(2) Frazier, B. A.; Williams, V. A.; Wolczanski, P. T.; Bart, S.; Meyer, K.; Cundari, T. R.; Lobkovsky, E. B. C-C Bond Formation and Related Reactions at the CNC Backbone in (smif)FeX (smif = 1,3-di-(2-pyridyl)-2-azaallyl): Dimerizations, 3 + 2 Cyclization, and Nucleophilic Attack; Transfer Hydrogenations and Alkyne Trimerization (X = $N(TMS)_2$, dpma (di-(2-pyridyl-methyl)-amide)). *Inorg. Chem.* **2013**, *52*, 3295−3312.

(3) Frazier, B. A.; Wolczanski, P. T.; Keresztes, I.; DeBeer, S.; Lobkovsky, E. B.; Pierpont, A. W.; Cundari, T. R. Synthetic Approaches to $(smif)_2Ti$ (smif = 1,3-di-(2-pyridyl)-2-azaallyl) Reveal Redox Non-Innocence and C-C Bond-Formation. *Inorg. Chem.* **2012**, *51*, 8177−8186.

(4) Morris, W. D.; Wolczanski, P. T.; Sutter, J.; Meyer, K.; Cundari, T. R.; Lobkovsky, E. B. Iron and Chromium Complexes Containing Tridentate Chelates Based on Nacnac and Imino- and Methyl-Pyridine Components: Triggering C-C(X) Bond Formation. *Inorg. Chem.* **2014**, *53*, 7467−7484.

(5) Volpe, E. C.; Wolczanski, P. T.; Darmon, J. M.; Lobkovsky, E. B. Syntheses and Characterizations of α-Iminopyridine Compounds $(AlkylN = CHpy)_2Fe(L/X_n)$, and an Assessment of Redox Non-Innocence. *Polyhedron* **2013**, *52*, 406−415.

(6) Hulley, E. B.; Williams, V. A.; Morris, W. D.; Wolczanski, P. T.; Hernández-Burgos, K.; Lobkovsky, E. B.; Cundari, T. R. Disparate Reactivity from Isomeric $\{Me_2C(CH_2N = CHpy)_2\}$ and $\{Me_2C(CH = NCH_2py)_2\}$ Chelates in Iron Complexation. *Polyhedron* **2014**, *84*, 182−191.

(7) Williams, V. A.; Hulley, E. B.; Wolczanski, P. T.; Lancaster, K. M.; Lobkovsky, E. B. Pushing the limits of redox non-innocence: pseudo square planar $[\{\kappa^4\text{-}Me_2C(CH_2N = CHpy)_2\}Ni]^n$ (n = 2+, 1+, 0, −1, −2) favor Ni(II). *Chem. Sci.* **2013**, *4*, 3636−3648.

(8) Lindley, B. M.; Wolczanski, P. T.; Cundari, T. R.; Lobkovsky, E. B. 1st Row Transition Metal and Lithium Pyridine-ene-amide Complexes Exhibiting N- and C-Isomers and Ligand-based Activation of Benzylic C-H Bonds. *Organometallics* **2015**, *34*, 4656−4688.

(9) Hulley, E. B.; Heins, S. P.; Wolczanski, P. T.; Lancaster, K. M.; Lobkovsky, E. B. Azaallyl-derived ring formation via redox coupling in first row transition metals. *Polyhedron* **2019**, *158*, 225−233.

(10) Jacobs, B. P.; Wolczanski, P. T.; Lobkovsky, E. B. Oxidatively Triggered Carbon-Carbon Bond Formation in Ene-amide Complexes. *Inorg. Chem.* **2016**, *55*, 4223−4232.

(11) Heins, S. P.; Zhang, B.; MacMillan, S. N.; Cundari, T. R.; Wolczanski, P. T. Oxidative Additions to Ti(IV) in $[(dadi)^{4-}]$-$Ti^{IV}(THF)$ Involve Carbon-Carbon Bond Formation and Redox-Noninnocent Behavior. *Organometallics* **2019**, *38*, 1502−1515.

(12) Blanchard, S.; Derat, E.; Desage-El Murr, M.; Fensterbank, L.; Malacria, M.; Mouries-Mansuy, V. Non-Innocent Ligands: New Opportunities in Iron Catalysis. *Eur. J. Inorg. Chem.* **2012**, *2012*, 376−389.

(13) Caulton, K. G. Systematics and Future Projections Concerning Redox-Noninnocent Amide/Imine Ligands. *Eur. J. Inorg. Chem.* **2012**, *2012*, 435−443.

(14) Dzik, W. I.; van der Vlugt, J. I.; Reek, J. N. H.; de Bruin, B. Ligands that Store and Release Electrons During Catalysis. *Angew. Chem., Int. Ed.* **2011**, *50*, 3356−3358.

(15) Budzelaar, P. H. M. Radical Chemistry of Iminepyridine Ligands. *Eur. J. Inorg. Chem.* **2012**, *2012*, 530−534.

(16) van der Vlugt, J. I. Radical-Type Reactivity and Catalysis by Single-Electron Transfer to or from Redox-Active Ligands. *Chem. - Eur. J.* **2019**, *25*, 2651−2662.

(17) Berben, L. A.; de Bruin, B.; Heyduk, A. G. Non-innocent ligands. *Chem. Commun.* **2015**, *51*, 1553−1554.

(18) Lyaskovskyy, V.; de Bruin, B. Redox Non-Innocent Ligands: Versatile New Tools to Control Catalytic Reactions. *ACS Catal.* **2012**, *2*, 270−279.

(19) Munhá, R. F.; Zarkesh, R. A.; Heyduk, A. F. Group transfer reactions of d^0 transition metal complexes: redox-active ligands provide a mechanism for expanded reactivity. *Dalton Trans.* **2013**, *42*, 3751−3766.

(20) van Leest, N. P.; Epping, R. F. J.; van Vliet, K. M.; Lankelma, M.; van den Heuvel, E. J.; Heijbrink, N.; Broersen, R.; de Bruin, B. Single-Electron Elementary Steps in Homogeneous Organometallic Catalysis. *Adv. Organomet. Chem.* **2018**, *70*, 71−180.

(21) Hojilla Atienza, C. C.; Milsmann, C.; Semproni, S. P.; Turner, Z. R.; Chirik, P. J. Reveersible Carbon-carbon Bond Formation Induced by Oxidation and Reduction at at Redox-Active Cobalt Complex. *Inorg. Chem.* **2013**, *52*, 5403−5417.

(22) Regenauer, N. I.; Settele, S.; Bill, E.; Wadepohl, H.; Rosca, D.-A. Bis(imino)pyrazine-Supported Iron Complexes: Ligand-Based Redox Chemistry, Dearomatization, and Reversible C-C Bond Formation. *Inorg. Chem.* **2020**, *59*, 2604−2612.

(23) Lu, C. C.; Bill, E.; Weyhermüller, T.; Bothe, E.; Wieghardt, K. Neutral Bis(α-iminopyridine)metal Complexes of the First-Row Transition Ions (Cr, Mn, Fe, Co, Ni, Zn) and Their Monocationic

Analogues: Mixed Valency Involving a Redox Noninnocent Ligand System. *J. Am. Chem. Soc.* **2008**, *130*, 3181−3197.
(24) (a) McWilliams, S. F.; Bill, E.; Lukat-Rodgers, G.; Rodgers, K. R.; Mercado, B. Q.; Holland, P. L. Effects of N_2 Binding Mode on Iron-Based Functionalization of Dinitrogen to Form an Iron(III) Hydrazido Complex. *J. Am. Chem. Soc.* **2018**, *140*, 8586−8598. (b) Al-Afyouni, M. H.; Suturina, E.; Pathak, S.; Atanasov, M.; Bill, E.; DeRosha, D. E.; Brennessel, W. W.; Neese, F.; Holland, P. L. Spin Isomers and Ligand Isomerization in a Three-Coordinate Cobalt(I) Carbonyl Complex. *J. Am. Chem. Soc.* **2015**, *137*, 10689−10699.
(25) Patra, S. C.; Biswas, M. K.; Maity, A. N.; Ghosh, P. Osazone Anion Radical Complex of Rhodium(III). *Inorg. Chem.* **2011**, *50*, 1331−1338.
(26) Bousseksou, A.; Molnar, G.; Real, J. A.; Tanaka, K. Spin crossover and photomagnetism in dinuclear iron(II) compounds. *Coord. Chem. Rev.* **2007**, *251*, 1822−1833.
(27) Noble, A.; Anderson, J. C. Nitro-Mannich Reaction. *Chem. Rev.* **2013**, *113*, 2887−2939.
(28) Appel, A. C. M.; Hage, R.; Russel, S. W.; Tetard, D. WO 01/085717 A1, 15 November 2001.
(29) (a) Evans, D. F. The Determination of the Paramagnetic Susceptibility of Substances in Solution by Nuclear Magnetic Resonance. *J. Chem. Soc.* **1959**, 2003−2005. (b) Schubert, E. M. Utilizing the Evans Method with a Superconducting NMR Spectrometer in the Undergraduate Laboratory. *J. Chem. Educ.* **1992**, *69*, 62.
(30) Addison, A. W.; Rao, N. T.; Reedijk, J.; van Rijn, J.; Verschoor, G. C. Synthesis, structure, and spectroscopic properties of copper(II) compounds containing nitrogen−sulphur donor ligands; the crystal and molecular structure of aqua[1,7-bis(N-methylbenzimidazol-2′-yl)-2,6-dithiaheptane]copper(II) perchlorate. *J. Chem. Soc., Dalton Trans.* **1984**, 1349−1356.
(31) Allen, F. H.; Kennard, O.; Watson, D. G.; Brammer, L.; Orpen, A. G.; Taylor, R. Tables of Bond Lengths determined by *X*-ray and Neutron Diffraction. Part 1. Bond Lengths in Organic Compounds. *J. Chem. Soc., Perkin Trans. 2* **1987**, S1−S19.
(32) Zavitsas, A. A. The Relation between Bond Lengths and Dissociation Energies of Carbon-Carbon Bonds. *J. Phys. Chem. A* **2003**, *107*, 897−898.
(33) Gibson, V. C.; O'Reilly, R. K.; Wass, D. F.; White, A. J. P.; Williams, D. J. Iron complexes bearing iminopyridine and aminopyridine ligands as catalysts for atom transfer radical polymerisation. *Dalton Trans.* **2003**, 2824−2830.
(34) Shejwalkar, P.; Rath, N. P.; Bauer, E. New iron(II) a-iminopyridine complexes and their catalytic activity in the oxidation of activated methylene groups and secondary alcohols to ketones. *Dalton Trans.* **2011**, *40*, 7617−7631.
(35) (a) Butschke, B.; Fillman, K. L.; Bendikov, T.; Shimon, L. J. W.; Diskin-Posner, U.; Leitus, G.; Gorelsky, S. I.; Neidig, M. L.; Milstein, D. How Innocent are Potentially Redox Non-Innocent Ligands? Electronic Structure and Metal Oxidation States in Iron-PNN Complexes as a Representative Case Study. *Inorg. Chem.* **2015**, *54*, 4909−4926. (b) Zell, T.; Milko, P.; Fillman, K. L.; Diskin-Posner, Y.; Bendikov, T.; Iron, M. A.; Leitus, G.; Ben-David, Y.; Neidig, M. L.; Milstein, D. Iron Dicarbonyl Complexes Featuring Bipyridine-Based PNN Pincer Ligands with Short Interpyridine C-C Bond Lengths: Innocent or Non-Innocent Ligand? *Chem. - Eur. J.* **2014**, *20*, 4403−4413.
(36) (a) Matyjaszewski, K.; Xia, J. Atom Transfer Radical Polymerization. *Chem. Rev.* **2001**, *101*, 2921−2990. (b) Matyjaszewski, K. Atom Transfer Radical Polymerization (ATRP): Current Status and Future Perspectives. *Macromolecules* **2012**, *45*, 4015−4039. (c) Dadashi-Silab, S.; Matyjaszewski, K. Iron Catalysts in Atom Transfer Radical Polymerization. *Molecules* **2020**, *25*, 1648. (d) Lorandi, F.; Matyjaszewski, K. Why Do We Need More Active ATRP Catatysts? *Isr. J. Chem.* **2020**, *60*, 108−123.
(37) (a) Poli, R. Radical Coordination Chemistry and Its Relevance to Metal-Mediated Radical Polymerization. *Eur. J. Inorg. Chem.* **2011**, *2011*, 1513−1530. (b) Poli, R.; Allan, L. E. N.; Shaver, M. P. Iron-mediated reversible deactivation controlled radical polymerization. *Prog. Polym. Sci.* **2014**, *39*, 1827−1845.
(38) (a) Matyjaszewski, K.; Wei, M. L.; Xia, J. H.; McDermott, N. E. Controlled/"living" radical polymerization of styrene and methyl methacrylate catalyzed by iron complexes. *Macromolecules* **1997**, *30*, 8161−8164. (b) Simakova, A.; Mackenzie, M.; Averick, S. E.; Park, S.; Matyjaszewski, K. Bioinspired Iron-Based Catalyst for Atom Transfer Radical Polymerization. *Angew. Chem., Int. Ed.* **2013**, *52*, 12148−12151. (c) Wang, Yu.; Matyjaszewski, K. ATRP of MMA in Polar Solvents Catalyzed by $FeBr_2$ without Additional Ligand. *Macromolecules* **2010**, *43*, 4303−4305.
(39) Ando, T.; Kamigaito, M.; Sawamoto, M. Iron(II) chloride complex for living radical polymerization of methyl methacrylate. *Macromolecules* **1997**, *30*, 4507−4510.
(40) (a) O'Reilly, R. K.; Shaver, M. P.; Gibson, V. C.; White, A. J. P. α-Diimine, Diamine, and Diphosphine Iron Catalysts for the Controlled Radical Polymerization of Styrene and Acrylate Monomers. *Macromolecules* **2007**, *40*, 7441−7452. (b) O'Reilly, R. K.; Gibson, V. C.; White, A. J. P.; Williams, D. J. Five-coordinate iron(II) complexes bearing tridentate nitrogen donor ligands as catalysts for atom transfer radical polymerisation. *Polyhedron* **2004**, *23*, 2921−2928.
(41) Zhu, G.; Zhang, L.; Zhang, Z.; Zhu, J.; Tu, Y.; Cheng, Z.; Zhu, X. Iron-Mediated ICAR ATRP of Methyl Methacrylate. *Macromolecules* **2011**, *44*, 3233−3239.
(42) Chen, Z. H.; Ma, Y.; Wang, X. Y.; Sun, X. L.; Li, J. F.; Zhu, B. H.; Tang, Y. Winning Strategy for Iron-Based ATRP Using In Situ Generated Iodine as a Regulator. *ACS Catal.* **2020**, *10*, 14127−14134.
(43) (a) Fazekas, E.; Nichol, G. S.; Garden, J. A.; Shaver, M. P. Iron(III) Half Salen Catalysts for Atom Transfer Radical and Ring-Opening Polymerizations. *ACS Omega* **2018**, *3*, 16945−16953. (b) Allan, L. E N.; MacDonald, J. P.; Nichol, G. S.; Shaver, M. P. Single Component Iron Catalysts for Atom Transfer and Organometallic Mediated Radical Polymerizations: Mechanistic Studies and Reaction Scope. *Macromolecules* **2014**, *47*, 1249−1257. (c) Lake, B. R. M.; Shaver, M. P. Iron(II) beta-ketiminate complexes as mediators of controlled radical polymerisation. *Dalton Trans.* **2016**, *45*, 15840−15849.
(44) Wang, J.; Han, J.; Xie, X.; Xue, Z.; Fliedel, C.; Poli, R. $FeBr_2$-Catalyzed Bulk ATRP Promoted by Simple Inorganic Salts. *Macromolecules* **2019**, *52*, 5366−5376.
(45) Nakanishi, S.-i.; Kawamura, M.; Kai, H.; Jin, R.-H.; Sunada, Y.; Nagashima, H. Well-Defined Iron Complexes as Efficient Catalysts for "Green" Atom-Transfer Radical Polymerization of Styrene, Methyl Methacrylate, and Butyl Acrylate with Low Catalyst Loadings and Catalyst Recycling. *Chem. - Eur. J.* **2014**, *20*, 5802−5814.
(46) Gütlich, P.; Bill, E.; Trautwein, A. X. *Mössbauer Spectroscopy and Transition Metal Chemistry: Fundamentals and Applications*; Springer-Verlag: 2011; p 568.
(47) Dey, A.; Gordon, J. B.; Albert, T.; Sabuncu, S.; Siegler, M. A.; MacMillan, S. N.; Lancaster, K. M.; Moënne-Loccoz, P.; Goldberg, D. P. A Nonheme Mononuclear $\{FeNO\}^7$ Complex that Produces N_2O in the Absence of an Exogenous Reductant. *Angew. Chem., Int. Ed.* **2021**, *60*, 21558−21564.
(48) (a) McGrath, A. C.; Cashion, J. D. Goldanskii-Karyagin effect and induced fields in rare earth-transition metal stannides. *Hyperfine Interact.* **2007**, *168*, 1103−1107. (b) Reguera, E.; Yee-Madeira, H.; Demeshko, S.; Eckold, G.; Jimenez-Gallegos, J. Nature of the Observed Asymmetry in Mössbauer Spectra of Iron (2+) Hexacyanometallates (III). *Z. Phys. Chem.* **2009**, *223*, 701−711. (c) Varnek, V. A.; Lavre-nova, L. G. Analysis of asymmetry of the Mössbauer bands of Fe_xZn_{1-x}(4-amino-1,2.4-Triazole)$_3(NO_3)_2$ complexes with the spin transition $^1A_{1<}=^{>5}T_2$ proof of anisotropy of iron atom vibrations. *J. Struct. Chem.* **1995**, *36*, 97−103.
(49) Lipschutz, M. I.; Chantarojsiri, T.; Dong, Y.; Tilley, T. D. Synthesis, Characterization, and Alkyne Trimerization Catalysis of a Heteroleptic Two-Coordinate Fe^I Complex. *J. Am. Chem. Soc.* **2015**, *137*, 6366−6372.

(50) Brenna, D.; Villa, M.; Gieshoff, T. N.; Fischer, F.; Hapke, M.; von Wangelin, A. J. Iron-Catalyzed Cyclotrimerization of Terminal Alkynes by Dual Catalyst Activation in the Absence of Reductants. *Angew. Chem., Int. Ed.* **2017**, *56*, 8451−8454.
(51) Werncke, C. G.; Müller, I. The ambiguous behaviour of diphosphines towards the quasilinear iron(I) complex $[Fe(NSiMe_3)_2)_2]^-$ − between inertness, P-C bond cleavage and C-C double bond isomerisation. *Chem. Commun.* **2020**, *56*, 2268−2271.
(52) Polezhaev, A. V.; Liss, C. J.; Telser, J.; Chen, C.-H.; Caulton, K. G. A PNNH Pincer Ligand Allows Access to Monovalent Iron. *Chem. - Eur. J.* **2018**, *24*, 1330−1341.
(53) Ouyang, Z.; Du, J.; Wang, L.; Kneebone, J. L.; Neidig, M. L.; Deng, L. Linear and T-Shaped Iron(I) Complexes Supported by N-Heterocyclic Carbene Ligands: Synthesis and Structure Characterization. *Inorg. Chem.* **2015**, *54*, 8808−8816.
(54) Lin, C.-Y.; Fettinger, J. C.; Grandjean, F.; Long, G. J.; Power, P. P. Synthesis, Structure, and Magnetic and Electrochemical Properties of Quasi-Lnear and Linear Iron(I), Cobalt(I), and Nickel(I) Amido Complexes. *Inorg. Chem.* **2014**, *53*, 9400−9406.
(55) Ung, G.; Rittle, J.; Soleilhavoup, M.; Bertrand, G.; Peters, J. C. Two-Coordinate Fe^0 and Co^0 Complexes Supported by Cyclic (alkyl)(amino)carbenes. *Angew. Chem., Int. Ed.* **2014**, *53*, 8427−8431.

https://doi.org/10.1021/acs.inorgchem.1c01815
Inorg. Chem. 2021, 60, 18662−18673